Wound Healing Splinting Devices for Faster Access and Use

Andrew W. Miller[1], Alexa R. Anderson[1], Alejandra Suarez-Arnedo[1] and Tatiana Segura[1,2,3]

With the goal of studying skin wound healing and testing new drug treatments to enhance wound healing in rodent models, there is a clear need for improved splinting techniques to increase surgical efficiency and support routine wound monitoring. Splinted wound healing models humanize wound healing in rodents to prevent contraction and instead heal through granulation tissue deposition, increasing the relevance to human wound healing. Current technologies require suturing and heavy wrapping, leading to splint failure and cumbersome monitoring of the wound. In this study, we developed a splint with resealable cap system that provides ease of access for wound inspection, therapeutic treatment delivery, and routine wound imaging without the need to unwrap and wrap the animal. Meanwhile, to overcome the challenges associated with suturing, we also developed adherent splints that can be applied to both hairless or haired mice with minimal wrapping. Both technologies are expected to improve and encourage the adoption of splinted wound healing models.

Keywords: Imaging, Methods, Models, Techniques, Tools

JID Innovations (2025);**5:**100332 doi:10.1016/j.xjidi.2024.100332

INTRODUCTION

After skin injury, the body progresses through 4 stages of healing to either regenerate the damaged tissue or form a scar. These 4 stages are generally categorized into homeostasis, inflammation, proliferation, and remodeling. When this natural progression of wound healing is disrupted and the wound remains in the inflammatory stage, the wound becomes chronic, and wound closure and tissue deposition are severely limited (Bowler, 2002; Caley et al, 2015; Dreifke et al, 2015; Eming et al, 2014; Han and Ceilley, 2017; Howard et al, 2013; Kimmel et al, 2016; Koh and DiPietro, 2011; Larouche et al, 2018; Opdenakker et al, 2018; Shih et al, 2010; Tan et al, 2011). Impaired wound healing and the development of chronic wounds are a major healthcare burden, which primarily afflicts patients with diabetes and the aging population (Blakytny and Jude, 2006; Eming et al, 2010; Gary Sibbald and Woo, 2008; Han and Ceilley, 2017; Krisp et al, 2013; Löffler et al, 2013; Opdenakker et al, 2018; Siddiqui and Bernstein, 2010). To improve our understanding of these wounds and develop effective treatments, scientists rely on animal models in pigs or rodents to study wound healing. Whereas pig skin is the most comparable with human skin, rodent models are more commonly reported owing to their economic advantage (Fischer et al, 2023). However, rodents possess an underlying muscle layer called the panniculus carnosus, which is capable of closing wounds through contraction. Because humans lack this panniculus carnosus, their wound healing process relies on re-epithelialization for closure (Fischer et al, 2023; Galiano et al, 2004). Therefore, to study the re-epithelialization of murine skin, splinting wound models have been developed to hold the panniculus carnosus in place and prevent it from contracting to close the wound (Davidson et al, 2013).

The splinted wound model has been used widely since it was first described by Galiano et al (2004), which uses a rigid silicone ring placed around the circular wound and sutured in place. This method has proven successful in preventing wound closure through contraction, but it poses numerous challenges in practice. Suturing the splints in place is time intensive, particularly when placing numerous wounds on each animal or when performing large animal studies. In addition, each wound must be covered with a layer of Tegaderm to protect the wound and any applied therapeutic followed by wrapping the animal with either Tefla or Vetwrap dressing. These steps are vital to protect the wound, but the dressing of the wounds does not lend itself well to daily imaging or wound inspection.

Recent alternative splint designs (Figure 1 presents examples) (Davidson et al, 2013; Nuutila et al, 2016) show similar designs that also require heavy wrapping and dressing of the animal. For experiments where frequent imaging or application of compounds to the wound bed is needed, the current splinted wound healing technologies are not optimal, requiring extensive handling of the animal and leading to high splint failure rates from the sutures detaching. In this study, we present 2 splint technologies that allow for either rapid imaging and compound application without the need for wrapping of the animal or fast application without the need for sutures with a simple wrapping method.

[1]*Department of Biomedical Engineering, Duke University, Durham, North Carolina, USA;* [2]*Department of Neurology, Duke University School of Medicine, Durham, North Carolina, USA; and* [3]*Department of Dermatology, Duke University School of Medicine, Durham, North Carolina, USA*

Correspondence: Tatiana Segura, Department of Biomedical Engineering, Duke University, 534 Research Drive, Wilkinson Building Rm 313, Durham, North Carolina 27708-0281, USA. E-mail: Tatiana.segura@duke.edu

Abbreviations: aPDMS, adhesive polydimethyl siloxane; EO-PEI, ethoxylated polyethyleneimine; PDMS, polydimethyl siloxane

Received 19 April 2024; revised 7 October 2024; accepted 5 November 2024

Cite this article as: JID Innovations 2025;5:100332

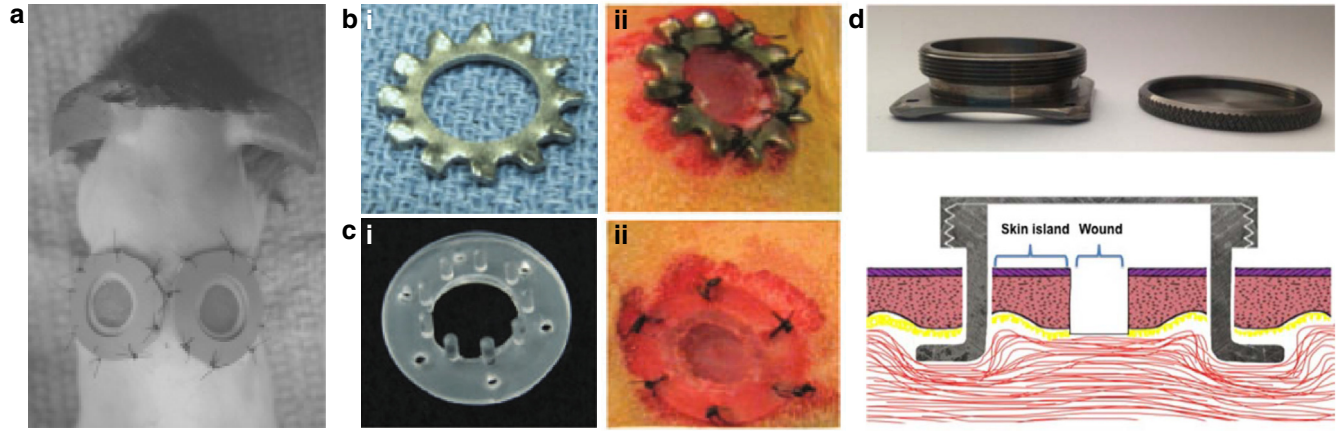

Figure 1. Existing splinting technology. (**a**) Traditional rubber or silicone splint as originally described in Galiano et al (2004). (**b**) Alternative splint design using a metal washer (Davidson et al, 2013). (**c**) Custom PDMS splint cast in a mold. It has short prongs protruding perpendicular to the classic doughnut base meant to prevent wound contraction by directly impeding growing skin (Davidson et al, 2013). (**d**) A titanium wound healing chamber containing a transdermal section, thus requiring a skin island (Nuutila et al, 2016). PDMS, polydimethyl siloxane.

The first splinting technology presented is constructed of a titanium base designed to be compatible with a plastic microcentrifuge tube cap (Figure 2b, inset ii). Beyond the splint performing its main duty of holding the wound open as it heals, the design goals for the titanium splint included sterilizable, reversibly and repeatedly sealable (ie, cap system), easily sutured to the animal, and reusable. One of the difficulties with the standard silicone or rubber splint is how much effort is required to push the suture needle through the elastic material. With such effort, complications are more frequent such as inefficient suture knot placement, insufficient amount of skin grabbed with the knot (too little or too much), and irregular tension on all sides of the wound leading to healing inconsistencies. The titanium splint overcomes all of these issues with its better temporary adherence to the skin with super glue (silicon splints cause the glue to bead/run off) as well as having designated windows for suturing that are large enough to facilitate surgical improvisation while maintaining structural integrity. Another advantage of using titanium over other splinted materials lies in its biocompatibility and nonallergenic nature, making this metal widely used as an implanted material in various biomedical applications (De Graaf et al, 2018). The cap is that of a microcentrifuge tube as we know them to be easily sterilizable through autoclave and low mass. This titanium splint requires no wrapping, and the cap can be easily removed for wound access.

The second splinting technology, called adhesive polydimethyl siloxane (aPDMS), is essentially an adhesive form of the standard silicone splint that sticks directly to the mouse skin and does not require sutures. Without the need for sutures, aPDMS is clearly the easiest way to splint a mouse wound and is incredibly effective. aPDMS is a polydimethyl siloxane (PDMS)—based material with ethoxylated polyethyleneimine (EO-PEI) added to disrupt the natural polymerization of the material, resulting in an improperly cured surface that is slightly wet or sticky that adheres well to most surfaces. Although there is a balance of how much EO-PEI to add, the optimal recipe results in a splint that negates any need for suturing as the splint itself adheres to the skin to provide equivalent tension in all directions around the wound.

RESULTS AND DISCUSSION

Titanium splint design

The design goals for the titanium splint included sterilizable, repeatedly sealable (ie, cap system), easily sutured to the animal, and reusable. The base material of titanium completes 2 of the 4 design criteria—sterilizable and reusable—by virtue of being a robust and tough metal. Achieving a suitable cap system and facilitating sutures proved to be more complicated. As shown in Figure 2, the titanium splint design can be broken into 3 regimes: the cap, the column, and the base plate. The cap and column must reversibly interlock and are thus paired throughout the iteration process; however, the base plate's sole responsibility is to accommodate sutures and could be independently designed and evaluated.

The first cap and column design (Figure 2a [insets i]) contained helical screw threads that were too small for the printer to reliably print for proper interlocking, and thus, the thread size was increased to what is shown in Figure 2a (insets ii). Despite proper interlocking, the weight of the cap brought the mass of the base plus cap to be greater than 2 g or about 10% of a typical C57BL/6J mouse aged 8–12 weeks. The large mass of the cap was deemed unsuitable because the mice would have difficulties carrying it and/or the sutures would pull through the skin under its out weight. To reduce the mass of the cap, 2 similar flat cap designs were attempted. These flat cap designs (Figure 2a [insets iii and iv] and b [insets iii and iv], respectively) showcase locking systems that use a piece of wire to lock the pieces together. In both designs, the wire does interlock the pieces together, but the flat caps were never able to sit flush on top of the column to create a seal. The sealing issue of the flat caps could be solved by combination of more precise manufacturing practices and using a gasketing material such as plastisol or other semihard plastics unpursued by us. The nonsealing nature of the flat caps precludes itself from being the final design. In observing the flat cap column simplicity and diameter, we acknowledged its similarity to the size of a microcentrifuge

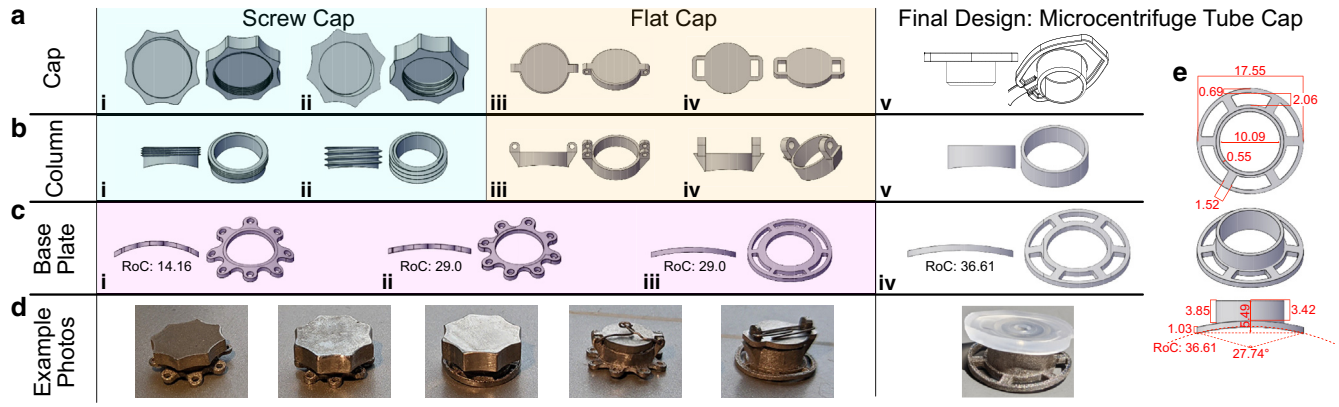

Figure 2. Titanium splint design iteration. (**a**) Insets i–v: Cap design iterations. (**b**) Insets i–v: Column design iterations designed to accommodate their corresponding caps in row. (**c**) Insets i–iv: Base plate design iterations. (**d**) Photos of exemplary prints throughout the iteration process. Specifications for the final base plate design are shown on the right; measurements are given in millimeters. RoC, radius of curvature.

tube cap, and it was decided to increase the column diameter to properly accommodate said cap, design shown in Figure 2b (inset v). This dramatically reduced the mass of the base plus cap mass by over 50% from >2 g to 0.95 g. There are 2 positive side effects of adopting the microcentrifuge tube cap design: first, the column design is simpler and with fewer crevices for bacteria accumulation/growth, and second, the disposable nature of the cap permits cap replacement at any time if it is ever observably dirty or otherwise compromised.

In designing the base plate, we had to include holes around the perimeter to permit suturing, and the plate itself must have a slight curve to it to better contour the curve of the mice's cylindrical body. The design concepts for the base plate are found in Figure 2c (insets i–iv), where initial designs show a spider-like suture-hole configuration that ultimately led to what we call the suture ring as well as slight changes to the radius of curvature throughout the process.

Conceptually, the spider-leg design works to equally space sutures around the perimeter, and the shape of the legs themselves would allow the surgeon to approach the suture hole from any angle. However, the suture holes ended up being so small that they would not permit the curved suture needle to pass through. We could have increased the size of each hole and corresponding leg, but this ended up requiring each leg to be quite close to one another, and ultimately, the design was abandoned for the much more capable suture ring. The suture ring is a semicontinuous hole surrounding the column where the surgeon themselves can choose where to suture the splint onto the animal, thus yielding a suture plate capable of surgical improvisation without sacrificing structural integrity. The radius of curvature was initially quite small to represent the curvature of the mouse back more accurately, but this aggressive radius of curvature proved to be inconsistent between animals, with some mouse bodies being more curved or flatter than others. To make the base plate more applicable to the majority of mice despite size differences, the radius of curvature was increased (flattened). Despite the mentioned prowess of the suture ring, the design in Figure 2c (inset iii) was not quite large enough to allow our suture needles to have completely free rotation while actively penetrating the suture ring so the suture hole had to be enlarged. Recall that the column diameter had to be increased from Figure 2b (insets iv and v) to accommodate the microcentrifuge tube cap; this provided the perfect opportunity to increase the size of the base plate altogether, thus achieving the desired increase in suture hole size.

The relative size of the final base plate in relation to the wound size allows the suture to be placed around 3–4 mm from the edge of the wound. This distance is generally similar to or larger than that of conventional sutured splints, where the ratio of the outer diameter of the splint to the diameter of the wound is 2:1 (Fischer et al, 2023) to 3:1(Wang et al, 2013). In our case, the ratio is 3.51:1, which represents a 17% increase in distance. This greater distance can help prevent any local inflammation caused by suturing from affecting the healing process (Dunn et al, 2013).

Ultimately, the design of the titanium splint using the microcentrifuge tube cap is rather simple, but its simplicity allows it to be easily attached to the mouse and used to repeatedly observe the wound healing process as discussed next.

Capped titanium splints allow for easy daily wound access

Quantifying the degree of wound closure over time is an important metric for assessing re-epithelialization, which relies on daily or periodic macroscopic imaging of the wound. Using the traditional splinted model, both the Vetwrap jacket and each individual wound's Tegaderm barrier must be removed to access the wound for imaging while the animal is under anesthesia. Imaging the wound requires frequent redressing, making the process time-consuming and labor-intensive. Jacketing the mice to preserve the surgical site's integrity is also a challenge; in fact, controlling the tightness of the wrapping is difficult and, if too tight, can restrict the mouse's ent or access to food/water. Furthermore, this process often puts tension on the sutures, causing them to tear from the skin. To overcome these challenges, we hypothesized that a splint with a window or a capping mechanism could be used to eliminate the repeated undressing and redressing of the wounds for routine inspection.

The removeable cap system with the titanium splint improved the efficiency of daily wound inspection as we eliminated several steps of undressing and redressing as required in the silicone splints. By minimizing mouse handling with the use of the titanium splints, we observed fewer incidences of tugging or pulling on the splint/wound. Daily images and their respective wound traces (Figure 3c–e) indicated clear similarities between silicone and titanium splints in their ability to prevent wound contraction (Figure 3g). Both silicone and titanium splints maintained a more rounded wound shape than unsplinted controls with aspect ratios being closer to 1 at day 7 (Figure 3j). The aspect ratio of 1 indicates equal tension on all sides of the wound to signify effective splinting. Not only does splinting impact the epithelial layer of skin, but it also impacts the size of the dermis, which we visualized in the histological sections of the wounds in Figure 3f. The cross-sectional area of the dermis allowed us to visualize greater dermis closure for unsplinted wounds than for wounds splinted with either silicone or titanium, quantified in Figure 3i.

Our splinted titanium design with a removable cap prevents direct contact with the wound, thus minimizing mechanical

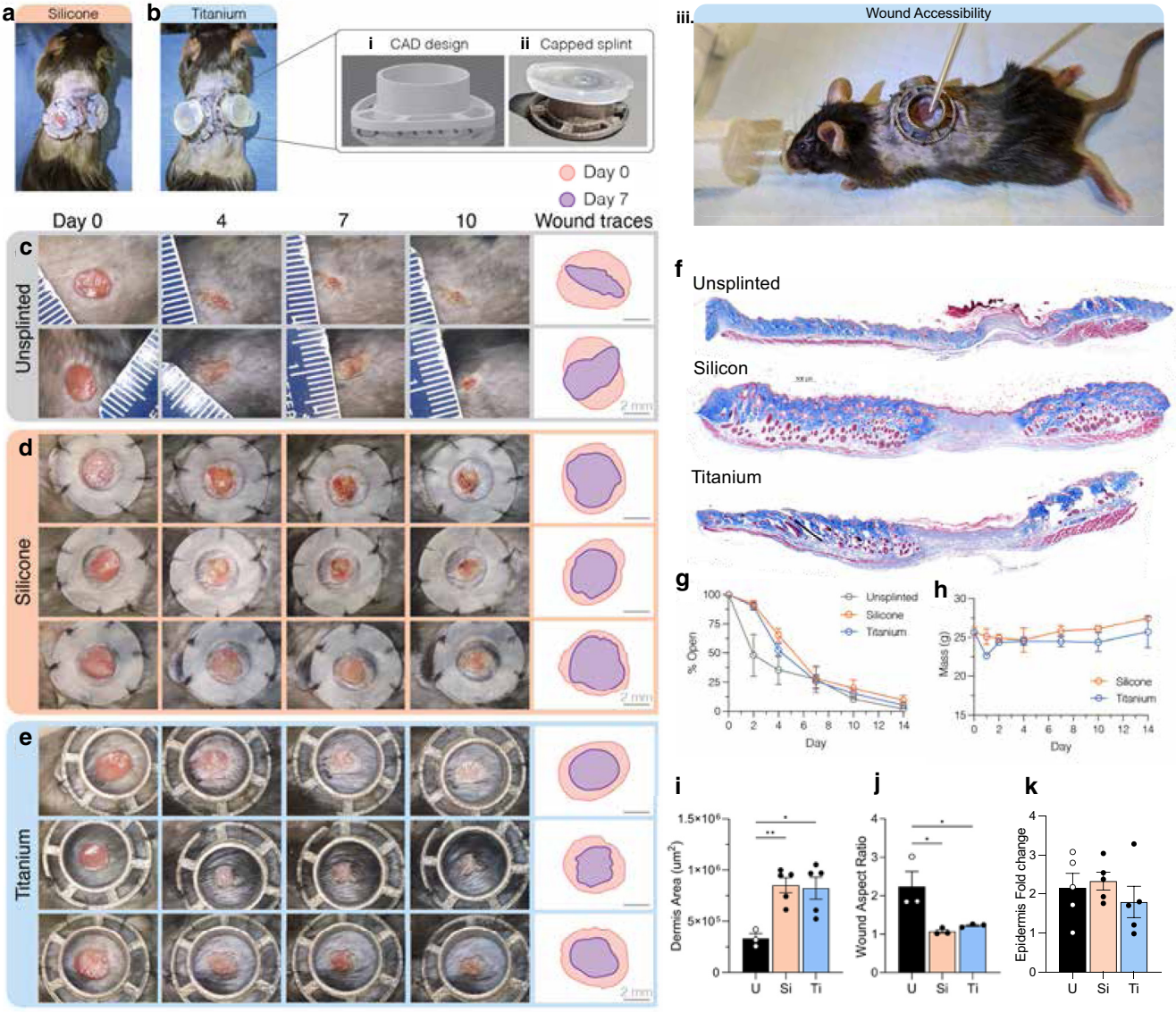

Figure 3. Titanium versus silicon splint performance in vivo. (**a**) Macroscopic image of a mouse with 2 wounds splinted with silicone splints. (**b**) Macroscopic image of a mouse with 2 wounds splinted with titanium splints showing (inset i) the CAD and (inset ii) capping ability. (**c**–**e**) Daily images of representative wounds from each condition with wound traces for each on days 0 and 7 overlapped in the rightmost column. Bar = 2 mm. (**f**) Cross-sectional skin sections at approximately the same depth containing the wounds from each condition, stained with Masson's trichrome stain. Bar = 500 μm. (**g**) How open each wound is with respect to itself (self-normalized); mean ± SEM, n = 5 wounds. (**h**) The masses of mice over time with each of the splinting conditions; mean ± SEM, n = 3 mice. (**i**) Dermis area measured from the lighter-colored, newer collagen found in representative sections of wounds at approximately the same depth into the wound; mean ± SEM, n = 5 wounds. (**j**) Wound aspect ratio calculated on the basis of the day-7 wound outlines in Figure 2c–e, using the longest contained line divided by the length of its perpendicular, shorter line; mean ± SEM, n = 3 wounds. (**k**) Epidermal fold change at wound margins compared with that at adjacent unwounded skin; mean ± SEM, n = 5 wounds. Statistics were generated using 1-way ANOVA with posthoc Tukey's test for multiple comparisons; $\alpha = 0.05$. CAD, computer-aided design.

contraction without imparting re-epithelialization during wound healing. To validate that our design does not adversely affect the wound bed, we quantified the fold change in epidermal thickness of the wound compared with that of adjacent unwounded skin. This metric is relevant because epidermal thickness is associated with keratinocyte proliferation during wound healing and the inflammatory response (Jabeen et al, 2019). Epidermal hyperplasia, commonly observed in injured skin, has been linked to inflammation, particularly to macrophage activity and the secretion of epidermal GFs (Koh and DiPietro, 2011). Our quantification results (Figure 3k) demonstrated no significant difference in epidermal thickness between unsplinted wounds, silicon-splinted wounds, and our titanium-splinted system. This finding confirms the suitability of our system in preventing wound contraction without influencing the wound bed or the overall progression of wound healing.

One consideration when using the larger titanium splint design versus the silicone splint was the additional mass added to each mouse. Each titanium splint added approximately 0.95 g per mouse. We hypothesize that the initial decrease in mass of the animals with titanium splints on day 1 was a result of this added weight (Figure 3h); however, the animal weights recovered and were comparable with the weights of those with silicone splints over the remaining 13 days. As a proof of concept, we printed the capped splint design using heat-resistant nylon rather than titanium to reduce the splint mass to 0.33 g, but this material alternative should be assessed for durability prior to use.

Through this work, we explored numerous approaches to improve surgical splints and techniques to increase the efficiency and accessibility of murine wound healing models. Wound healing studies with traditional silicone splints are surgically intensive and require repetitive undressing and redressing of the wounds for wound monitoring. To overcome these limitations, we developed a capped titanium splint, which was easier to suture, and maintained splinting action over 14 days. This design offered a resealable cap system for easy access to the wound for routine imaging and wound monitoring. However, considering the prototype nature of this process, several improvements can be made to the splint with the introduction of mass production techniques such as alternative tough materials such as nylon, polished surfaces to future prevent risk of microorganism attachment to the splint, or even proprietary plastic caps with slightly smaller diameter to reduce the required size of the column.

Adhesive properties granted to PDMS through chemical disruption of polymerization

During wound healing studies, suturing the splints accounts for the greatest portion of surgery time. Although the titanium splint design with a capped lid enabled easy access to wounds for daily imaging, this splint design still relied on suturing for securing the splint in place. The adhesive glue used when initially placing the splints prompted our hypothesis that an adhesive splint could abrogate the need for sutures to secure the splint in place. To create a splint out of an adhesive material, we modified the methods by Jeong et al (2016), which used EO-PEI to disrupt the crosslinking of the elastomer for making PDMS (Figure 4a). The addition of EO-PEI resulted in irregular polymerization densities to create a softer, highly adhesive material (Figure 4b and c) (Jeong et al, 2016). It is important to note that PDMS is widely recognized as safe and biocompatible for use on the skin, with a long history of biomedical applications (Juárez-Moreno et al, 2015; Miranda et al, 2021). Although some ethoxylated compounds have been associated with potential allergenic activity (Karlberg et al, 2003), there is limited evidence of such effects, specifically for EO-PEI in this context. Furthermore, PDMS and other silicone-based materials have been extensively used in medical applications for preventing scarring (Shirakami et al, 2020), underlining their suitability for skin contact in various therapeutic scenarios.

Several concentrations of EO-PEI were explored for creating an optimal aPDMS recipe to use as a splint. We performed a tack test using a custom-designed sample plate on a rheometer to determine the level of adhesiveness in aPDMS upon varying the EO-PEI concentration (Supplementary Videos S1–S3). The pull-off force was greatest in magnitude for the low EO-PEI concentration (1.55 μM), but the force occurred over the shortest time scale, resulting in the least 'sticky' formulation (Figure 4d). On the other hand, the high EO-PEI concentration (1.84 μM) generated the lowest pull-off force, but it occurred over the longest time period, resulting in the 'stickiest' formulation (Figure 4d). At this concentration, we observed the aPDMS making 'legs' that traveled with the rheometer testing plate as it moved away from the sample. These legs produced a smaller negative normal force that acted over a much longer timescale to elongate the normal force spike. We also observed residual aPDMS on the plate surface after testing. To avoid leaving residue on the skin, we opted for a moderate EO-PEI concentration of 1.69 μM. At this concentration, EO-PEI sufficiently disrupted the network to permit polymer relaxation and create a highly adhesive material that did not break nor leave behind a residue. We also reported the area under each curve normalized to the absolute value of the curve's minimal negative pull-off force to compare aPDMS with different EO-PEI concentrations (Figure 4e). The green shaded box highlights the range for the 1.69 μM EO-PEI concentration that created an effective level of adhesive without leaving residue.

We demonstrated the efficacy of aPDMS for adhering to both human skin as a proof of concept (Figure 4c [inset iii]) as well as different strains of mice over time. The aPDMS remained robustly adherent to hairless (SKH-1) mice over approximately 10–14 days before needing to be replaced. For haired mice, the aPDMS did not adhere to the skin unless cleanly shaved; however, when the skin was shaved, the aPDMS effectively adhered to the skin over approximately 8–12 days until the hair regrew. The traditional silicone splints and titanium splints should be used for long wound healing studies (>14 days) in haired mice owing to the clear challenge of using aPDMS in the presence of hair. However, we hypothesized that in hairless mice, aPDMS splints would maintain adhered to the skin without requiring sutures.

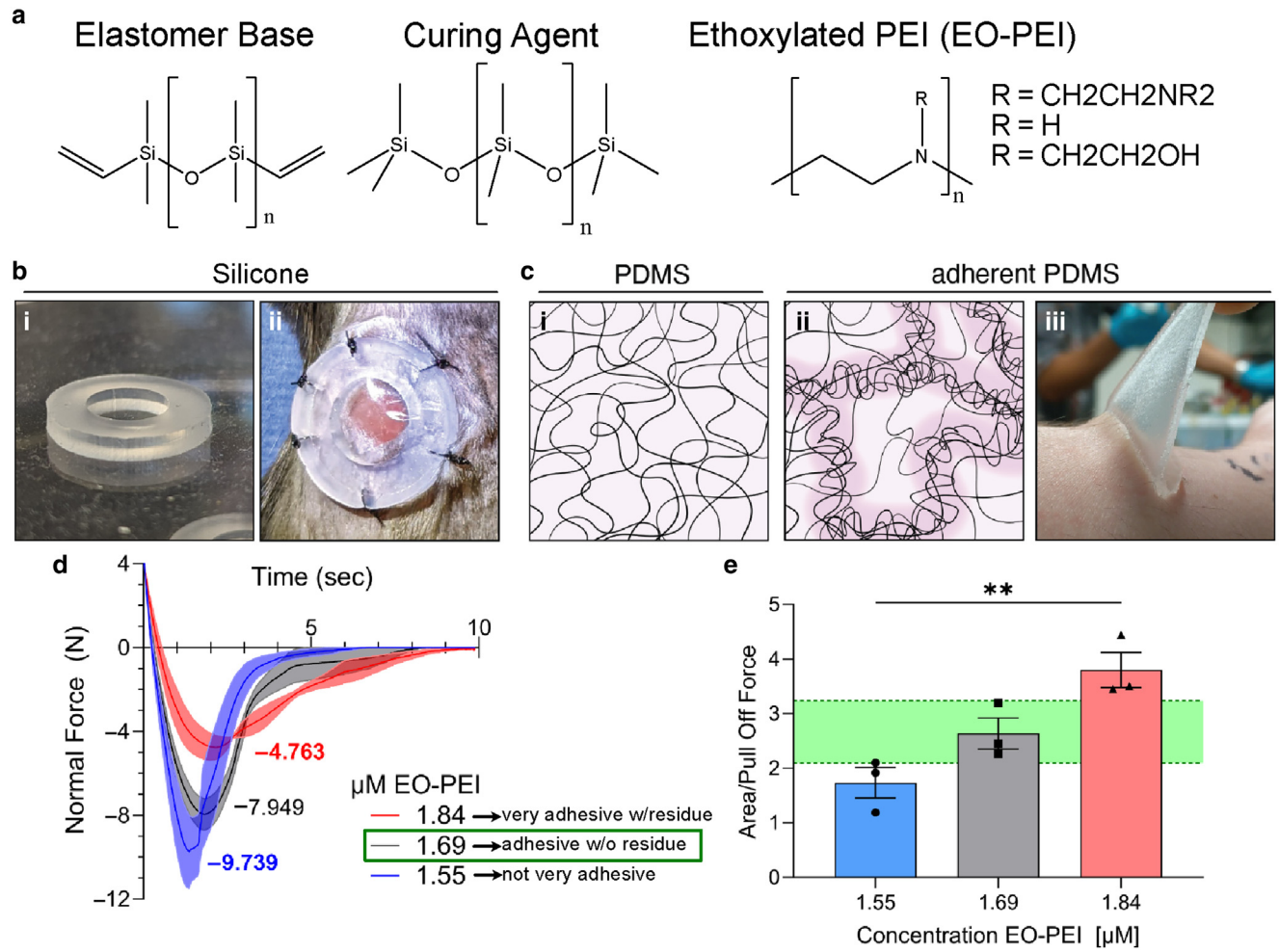

Figure 4. aPDMS composition and tack (adhesiveness). (**a**) Molecular structures of the polymer components. (**b, c**) Illustrations of the PDMS polymer network with and without EO-PEI and real-world applications of both materials. Illustration was adapted from Jeong et al (2016) with permission from Wiley-VCH Verlag. (**d**) Rheological data from a tack test of different aPDMS compositions with their respective minimal normal forces labeled; mean ± SEM, n = 3 different creations of aPDMS. Blue/low condition contains 1.55 μM of EO-PEI, black/optimal condition contains 1.69 μM of EO-PEI, and red/high condition contains 1.84 μM of EO-PEI. (**e**) AUC normalized to normal force; mean ± SEM, n = 3 different creations of aPDMS. The green zone represents ± 1 SD from 1.69 μM condition. Statistics were generated using 1-way ANOVA with posthoc Tukey's test for multiple comparisons; $\alpha = 0.05$. aPDMS, adhesive polydimethyl siloxane; AUC, area under the curve; EO-PEI, ethoxylated polyethyleneimine; PDMS, polydimethyl siloxane.

Suture-free aPDMS splints prevent wound contraction and are easily applied to wounds as a sticker

After creating adhesive splints with aPDMS, we evaluated their splinting ability and durability against the field standard silicone splints in a wound healing model. Without the need for sutures, surgery time decreased from approximately 10–15 minutes per wound to only 10–15 seconds per wound, thus vastly increasing the procedure efficiency. Figure 5a shows an examplary mouse from this set of experiments with one of each splint type and an athletic tape "jacket." The arrow in Figure 5a points out the protruding suture knots from the silicone splint that disrupted the Tegaderm film and prevented proper wound coverage. The sutures also often snagged on the animal jackets, which led to the tugging/pulling on splints. Without sutures, the aPDMS splints improved the attachment of Tegaderm to seal the splint and prevented external interference while maintaining a moist wound environment. More than this, aPDMS splints were easily replaceable. In this experiment, wounds were examined every 2–4 days, and when even a small part of the aPDMS splint started to lift off, it was simple to gently remove the old splint and replace it with a new splint.

In addition to the enhanced practicality of using sticker-like aPDMS splints for wound healing studies, the splinting ability of aPDMS splints was also comparable with that of silicone splints. Daily images and their respective wound traces (Figure 5c and d) indicated clear similarities between silicone and aPDMS splints in their ability to prevent wound contraction over 14 days (Figure 5f). There was no significant difference in the dermis area of the splinted wounds, and the wound aspect ratio for each type of splint was approximately 1.0 on day 7 (Figure 5i). Epidermal fold change quantification (Figure 5j) demonstrated no significant differences between unsplinted, silicone-splinted, and aPDMS-splinted wounds in the ratio of epidermal thickness of the wound compared with that of adjacent unwounded skin. This finding validates that similar to our titanium system, the aPDMS in SKH1 mice did not influence the wound bed or wound healing progress.

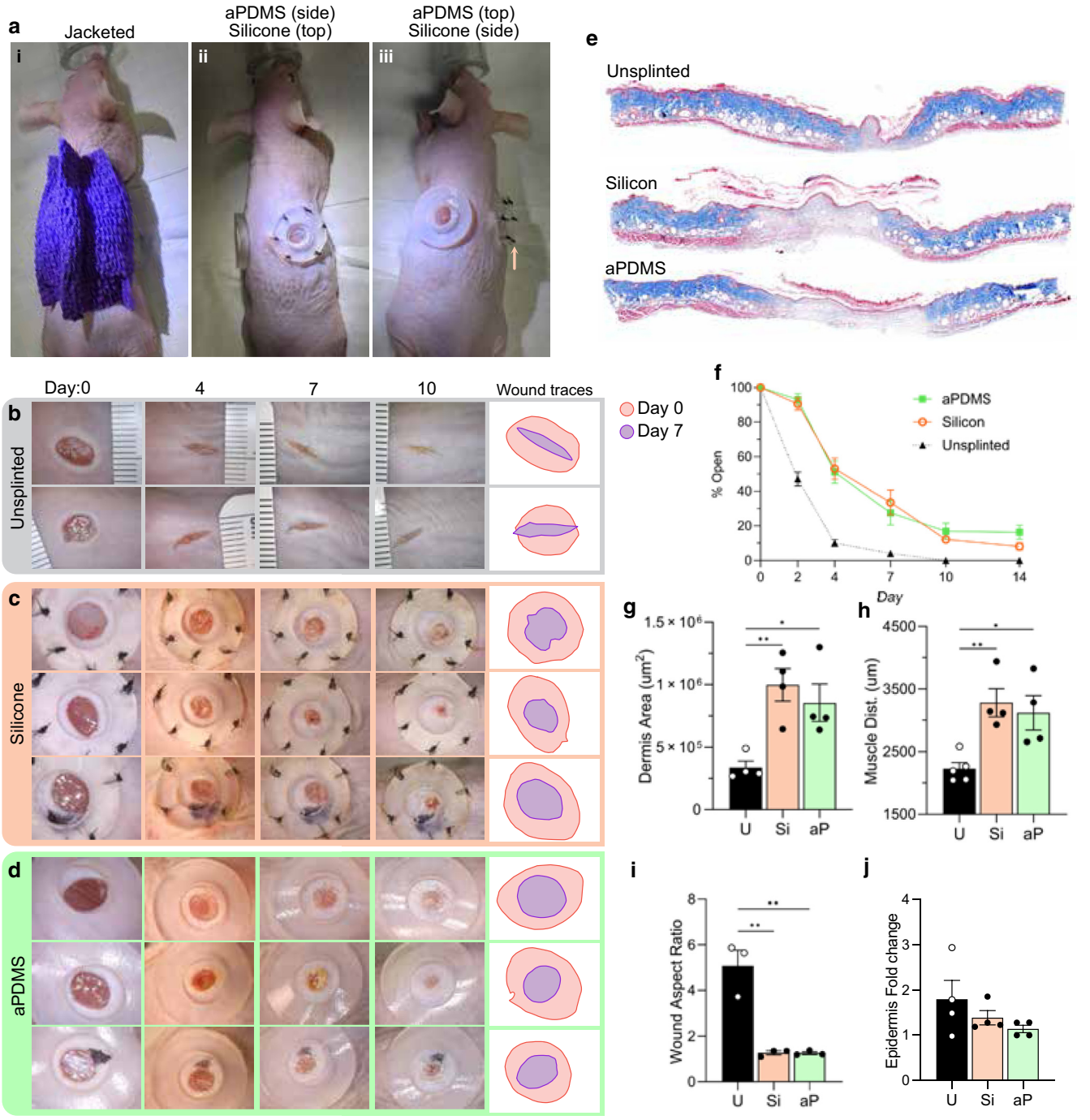

Figure 5. aPDMS versus silicon splint performance in vivo. (**a**) Pictures of the jacketed mouse and both splinted conditions. The arrow in **a** (inset iii) indicates suture knot protrusion from the splint's surface. (**b**–**d**) Daily images of representative wounds from each condition with wound traces for each on days 0 and 7 overlapped in the rightmost column. Bar = 2 mm. (**e**) Cross-sectional skin sections containing the wounds from each condition, stained with Masson's trichrome stain. Bar = 500 μm. (**f**) How open each wound is with respect to itself (self-normalized); mean ± SEM, n = 4 wounds. (**g**) Dermis area measured from the lighter-colored, newer collagen found in representative sections of wounds at approximately the same depth into the wound; mean ± SEM, n = 4 wounds. (**h**) Distance between the separated subcutaneous muscle—panniculus carinosus—at the approximate same depth into the wound; mean ± SEM, n = 4 wounds. (**i**) Wound aspect ratio calculated on the basis of the day-7 wound outlines in Figure 4b–d, using the longest contained line divided by the length of its perpendicular, shorter line; mean ± SEM, n = 3 wounds. (**j**) Epidermal fold change at wound margins compared with that at adjacent unwounded skin; mean ± SEM, n = 4 wounds. Statistics were generated using 1-way ANOVA with posthoc Tukey's test for multiple comparisons; $\alpha = 0.05$. aPDMS, adhesive polydimethyl siloxane.

Interestingly, across the 4 histological metrics quantified, both the silicone-splinted and aPDMS-splinted wounds showed smaller variances than the unsplinted wounds. This observation validates that our technologies maintain the reproducibility of wound healing outcomes in the excisional splinted model (Galiano et al, 2004). The reduced variability

in splinted wounds underscores the model's improved consistency and reliability for wound healing studies.

Although the capped titanium splint improved wound access, this design still required suturing to secure the splint in place. To overcome the challenges associated with suturing, we developed adherent splints composed of PDMS alternatively cured with EO-PEI, called aPDMS. These aPDMS splints effectively adhered to hairless mice skin and prevented skin contraction as effectively as the traditional silicone splints. More than this, wound moisture was easier to maintain using aPDMS splints because the Tegaderm seal was not disrupted by protruding sutures. The use of these aPDMS splints also drastically decreased the time of the surgical procedure. Part of this huge decrease in time required per wound is the much lower skill required to apply these 'sticker' splints. This technology will allow less skilled researchers to perform in vivo wound healing studies without fear of accidental suture failure or infection resulting from poor surgical skills. With the establishment of this more reliable, easily accessed platform for research, we hope to see more agreement between different research laboratories and ultimately enable the development of better wound healing therapies.

This manuscript presents 2 splinted murine models specifically adapted for the hair-bearing C57BL/6J mice (using titanium splints) and the naturally hairless but immunocompetent SKH1-Elite mice (using aPDMS splints). These models build upon the excisional wound healing model described by Galiano et al (2004) demonstrating significant improvements in overcoming technical challenges associated with traditional splinted murine models. Notably, our approach reduces surgery time, simplifies monitoring, allows free mobility in the mice (Supplementary Videos S4 and S5), and decreases the level of skill required from researchers performing the surgery. Although we followed Galiano et al (2024)'s guidelines, using a biopsy punch to create wounds on the mouse dorsum between the scapular and sacral regions, we did not ensure that all wounds were in the exact same subanatomical region. As highlighted by Yao et al (2014), animal activity can influence wound healing, especially when wounds are located at the top or middle of the back. Nevertheless, our quantitative measurements reported in Figures 3 and 5 demonstrate that both our models are comparable with classical splinted models in terms of reproducibility. Importantly, they significantly reduce the variance observed in unsplinted wounds. This enhanced consistency underscores the value of our approaches in advancing wound healing research.

MATERIALS AND METHODS

Silicone splint fabrication

Silicone splints were punched out of a 0.08-inch-thick sheet of USP Class IV silicone using 14 and 7 mm biopsy punches for the outer and inner diameters, respectively (Firm Matte Silicone Sheeting, catalog 70P001-100-080). The silicone splints were autoclaved with other surgical equipment prior to use.

Titanium splint fabrication

The titanium splints were designed in Autocad, exported to .stl files, and sent to the Gall laboratory at Duke University for 3-dimensional printing using a 3-dimensional systems DMP ProX 320 printer with Ti6Al4V Grade 23 spherical powder (Kelly et al, 2019). Although only 1 design was evaluated in vivo in this work, several design concepts and iterations were required to arrive at this final design, shown in Figure 2. Upon receiving the printed splints, the pieces were manually processed (not shown) using a Dremel and a variety of sanding and buffing bits until the mouse side of the splint base was smooth to touch. The titanium base was autoclaved with other surgical equipment prior to use.

The microcentrifuge tube caps were sourced from Fisher Scientific (catalog 1615-5510). The caps were cut off using an exacto-knife and autoclaved alongside other surgical tools. Despite these tubes being sterile out of the bag, it is important to autoclave the caps because the plastic slightly deforms during autoclaving, and this is the right size that will fit into the designed titanium base.

aPDMS fabrication

aPDMS uses the SYLGARD 184 Silicone Elastomer Kit ordered directly from Dow Chemical with added EO-PEI, 80% ethoxylated, and 37wt% in water (Sigma-Aldrich, catalog number 306185-100G). aPDMS maintains the normal ratios of 10 g base elastomer to 1 g curing agent as described in the SYLGARD 184 Silicone Elastomer Kit. After measuring out the desired base and curing agent mass, a positive displacement pipette was used to add EO-PEI solution to achieve the desired concentration of EO-PEI. For example, to fill a 10 × 10 cm square petri dish resulting in aPDMS of approximately 1.5 mm height and optimal adhesiveness, we combined 17 g base elastomer with 1.7 g curing agent and then added 87.5 μl of the EO-PEI. The mixture was then stirred vigorously and thoroughly for 60 seconds, poured into curing dish or other mold, and degassed under vacuum for 15 minutes. After degassing, the curing dish or mold was placed into a 60 °C oven overnight for 16−18 hours, with the sticky side covered by the petri dish lid but open to air. Considering that EO-PEI is meant to disrupt the curing process slightly, one can expect some irregularities with the curing process. The overnight curing step may not be enough time to fully cure the aPDMS, and it can remain almost liquid like. If this occurs, longer curing times or higher temperatures should be attempted. If curing does not occur in the next 1−2 days, it will never cure and will need to be remade. Both the SYLGARD 184 Silicone Elastomer Kit and EO-PEI are subject to environmental oxidation over time. It was observed in our studies that fresher components were more consistent in producing viable aPDMS; thus, ingredients should be replaced every 4−6 months to ensure consistency. The resulting aPDMS should be slightly softer than normal PDMS and incredibly sticky to the touch but without any visible residue left behind after removal. Importantly, aPDMS is only adhesive on the air-exposed side; the mold side will be glossy and negligibly adhesive.

To create splints, the aPDMS was kept in its original curing petri dish where we then used 2 biopsy punches to achieve the recognizable doughnut style shape; outer diameter is 14 mm, and inner diameter is 7 mm. Sterile practices were used during the punching. To sterilize the splints, the excess aPDMS (from punches) was removed, and the splints were washed with 70% ethanol briefly for 1−2 minutes before the excess ethanol solution was then poured off. The splints were then allowed to airdry under UV light before putting a lid on the petri dish and sealing the lid's air gap with parafilm. aPDMS remains adhesive for 2−4 weeks, less if exposed to dust or high temperatures.

aPDMS tack testing

The adhesive properties of aPDMS were measured using the Anton Paar Physica MCR 301 and an altered form of its preloaded tack test experiment setup in its software, RheoCompass. Before testing aPDMS directly with the machine, a custom stage was designed and 3-dimensional printed in polylactic acid, so that the aPDMS could be cured in a rheometer-mountable dish. This stage was required because aPDMS is incredibly sticky on one side, and thus, if it were taken out and placed onto another surface, the sticky top surface would adhere to the measuring device, and only the glossy, nonadhesive bottom surface interaction would be measured. Casting aPDMS in the measurement stage ensures that the material is locked into position where the top, adhesive surface is free to adhere and dissociate from the measuring device. The measuring device was a roughened 15-mm diameter parallel plate that descended onto the adhesive top surface of the aPDMS to a force of approximately 5−6 N. The plate is then lifted at a constant velocity of 100 μm/second, whereas the rheometer measured the downward pulling force of the adhesive surface to create the pull-off curves found in Figure 4d.

Surgery: mouse preparation and wounding

All animal experiments were performed in accordance with the approved Duke Institutional Animal Care and Use Committee protocol. After knockdown with isoflurane, C57BL/6J mice dorsal fur was removed using hair clippers. Without back hair, both C57BL/6J and the naturally hairless but immunocompetent SKH1-Elite mice were processed similarly. Both types of mice were prepared for dorsal skin surgery with 3 rounds of alternating iodine and isopropanol towelette washes with a final, extra isopropanol towelette wash to ensure no remaining iodine. Analgesic, Burprenorphine ER-LAB from ZooPharm (dose 0.5 mg/kg), was then properly administered to the subcutaneous area just above the shoulders (low neck) of the mice. Two wounds at a time were made in the dorsal skin by first tenting the skin and then forcing a 5-mm diameter biopsy punch perpendicularly through the tented skin (both layers) and into a wood tongue depressor. It is important to clarify that, as shown in Figures 3a and 5a, we used a biopsy punch to create 2 wounds on the mouse dorsum. These wounds were positioned symmetrically, one on each side of the midline, in the area between the scapular and sacral regions of the mouse back. This procedure follows the protocol for creating excisional murine wounds as described by Galiano et al (2004). This approach ensures consistency in wound placement and allows for comparison between experimental groups (Galiano et al, 2004).

Surgery: silicone splint application

After wounding, superglue (Krazy glue) was used to temporarily adhere the silicone splints centered around the wound. A needle driver and forceps were used alongside a reverse cutting 12 mm 3/8c suture needle with nylon monofilament line to place 6 suture knots spaced equidistant around the outer edge of the splint (Surgical Specialties, catalog 931B). Nylon monofilament was used for suture over other suturing materials because it is one of the most common materials for suturing cutaneous surgeries (Callahan et al, 2017), has been widely used in the literature for splinted excisional murine models (Hagerott et al, 2020; Wang et al, 2013), and has been reported to produce the least inflammatory response than other materials (Trail et al, 1989). The sutures penetrated both the silicon splint and a small tuft of normal mouse skin to ensure attachment at all 6 knot locations. The suture knots were composed of an initial triple overhand knot followed by 2 alternating direction double overhand knots with the excess line cut off. After the splint was attached, circular Tegaderm (diameter = 12 mm) was carefully peeled and applied to the to the splint to seal the wound and splint. Vetwrap was used to create a jacket covering the entire midsection of the mouse to prevent the mice from chewing on the sutures/splints and keep the sutures secured.

Surgery: titanium splint application

After wounding, superglue was applied to the skin side of the titanium base plate and placed on the skin centered around the wound. A total of 6−8 sutures (same suture needle and line) were equally spaced around the circumference of the base plate. The sterilized microcentrifuge tube cap was placed into the base plate to seal the wound. Most microcentrifuge tube caps have a long piece of plastic overhang for fingers to grip to open closed tubes, so we recommend putting this overhang facing toward the center of the back to prevent mice from using the overhang as leverage for cap removal.

Surgery: aPDMS splint application

After wounding, forceps were used to carefully peel the aPDMS splint off the curing petri dish (recall, the adhesive side faces up, toward the air) and placed centered around the wound, with the adhesive side touching the skin. The splints were gently pressed to ensure proper adherence. After attaching the splint, circular Tegaderm (diameter = 12 mm) was applied to the splint to seal the wound. Vetwrap jacket was applied as previously described.

Daily imaging

With day 0 being surgery day, daily checkups are encouraged, but wound imaging typically occurs on days 0, 2, 4, 7, 10, and 14. Imaging requires exposure of the wound and thus removal of different layers of dressing for each condition. Images were collected using Celestron's Handheld Digital Microscope Pro (catalog 44308) alongside its compatible software, MicroCapture Pro. Although rare, if an aPDMS splint appeared to slightly lift off the skin, a new aPDMS splint was applied.

Skin collection, embedding, and blinding

On day 14, mice were humanely killed through carbon dioxide suffocation followed by decapitation. The remaining sutures were cut and removed from the skin, and aPDMS was peeled away. The entirety of the dorsal skin was removed using surgical scissors and placed onto a flat cutting surface. A circle of skin was excised centered around the wound using a 1-cm diameter biopsy punch. The skin was placed flatly in a tissue sample cassette and incubated 4% paraformaldehyde (in PBS) overnight at 4 °C. The fixed samples were transferred to 70% ethanol prior to embedding in paraffin wax. All samples were blinded for analysis.

Sectioning and staining

Embedded samples were sectioned using an Epredia HM355S in manual mode. Sections were collected in the following structured series: 6 slides with 2−3 sections (5 μm in thickness) on each slide followed by the removal of 100 μm of sample prior to starting the next series. Slides from the same series location were selected from each condition and stained with Masson's trichrome, according to the manufacturer's instructions.

Imaging and analysis

Stained sections were imaged using ×20 magnification on the Zeiss Axioscan. Image Lookup Tables were manually adjusted to contain all signal strength and exclude intensity regions without any signal. Images were exported to .tif using 40% compression. ImageJ was used for color deconvolution and measuring the area of newly

deposited dermis/collagen (lighter blue compared with the native, darker blue).

Statistical analysis

Statistical difference among 3 conditions—no splint, silicone, or experimental—was determined by 1-way ANOVA with posthoc Tukey's test for multiple comparisons. Error bars are SEM. Comparisons containing only 2 datasets were compared using Welch's *t*-tests. Significance threshold used $\alpha = 0.05$.

Ethics statement

All animal experiments were performed in accordance with the approved Duke Institutional Animal Care and Use Committee protocol.

Data availability statement

Data is available via https://doi.org/10.7924/r4rn3ct2v.

ORCIDs

Andrew W. Miller: http://orcid.org/0000-0002-7444-8524
Alexa R. Anderson: http://orcid.org/0000-0002-8566-4310
Alejandra Suarez-Arnedo: http://orcid.org/0000-0001-9235-0910
Tatiana Segura: http://orcid.org/0000-0003-1569-8686

CONFLICT OF INTEREST

The authors state no conflict of interest.

ACKNOWLEDGMENTS

This research was supported by the National Institutes of Health under grants R01AI152568.

AUTHOR CONTRIBUTIONS

Conceptualization: AWM, TS; Data Curation: AWM, TS; Formal Analysis: AWM, AS-A; Funding Acquisition: TS; Investigation: AWM; Methodology: AWM, TS; Project Administration: TS; Resources: TS; Software: AWM; Supervision: TS; Validation: AWM; Visualization: ARA; Writing - Original Draft Preparation: AWM, ARA; Writing - Review and Editing: AWM, ARA, AS-A, TS

DECLARATION OF GENERATIVE ARTIFICIAL INTELLIGENCE (AI) OR LARGE LANGUAGE MODELS (LLMs)

The author(s) did not use AI/LLM in any part of the research process and/or manuscript preparation.

SUPPLEMENTARY MATERIAL

Supplementary material is linked to the online version of the paper at www.jidonline.org, and at https://doi.org/10.1016/j.xjidi.2024.100332.

REFERENCES

Blakytny R, Jude E. The molecular biology of chronic wounds and delayed healing in diabetes. Diabet Med 2006;23:594–608.

Bowler PG. Wound pathophysiology, infection and therapeutic options. Ann Med 2002;34:419–27.

Caley MP, Martins VL, O'Toole EA. Metalloproteinases and wound healing. Adv Wound Care (New Rochelle) 2015;4:225–34.

Callahan TL, Lear W, Kruzic JJ, Maughan CB. Mechanical properties of commercially available nylon sutures in the United States. J Biomed Mater Res B Appl Biomater 2017;105:815–9.

Davidson JM, Yu F, Opalenik SR. Splinting strategies to overcome confounding wound contraction in experimental animal models. Adv Wound Care (New Rochelle) 2013;2:142–8.

De Graaf NPJ, Feilzer AJ, Kleverlaan CJ, Bontkes H, Gibbs S, Rustemeyer T. A retrospective study on titanium sensitivity: patch test materials and manifestations. Contact Dermatitis 2018;79:85–90.

Dreifke MB, Jayasuriya AA, Jayasuriya AC. Current wound healing procedures and potential care. Mater Sci Eng C Mater Biol Appl 2015;48:651–62.

Dunn L, Prosser HC, Tan JT, Vanags LZ, Ng MK, Bursill CA. Murine model of wound healing. J Vis Exp 2013;75:e50265.

Eming SA, Koch M, Krieger A, Brachvogel B, Kreft S, Bruckner-Tuderman L, et al. Differential proteomic analysis distinguishes tissue repair biomarker signatures in wound exudates obtained from normal healing and chronic wounds. J Proteome Res 2010;9:4758–66.

Eming SA, Martin P, Tomic-Canic M. Wound repair and regeneration: mechanisms, signaling, and translation. Sci Transl Med 2014;6:265sr6.

Fischer KS, Litmanovich B, Sivaraj D, Kussie HC, Hahn WW, Hostler AC, et al. Protocol for the splinted, human-like excisional wound model in mice. Bio Protoc 2023;13:e4606.

Galiano RD, Michaels J 5th, Dobryansky M, Levine JP, Gurtner GC. Quantitative and reproducible murine model of excisional wound healing. Wound Repair Regen 2004;12:485–92.

Gary Sibbald R, Woo KY. The biology of chronic foot ulcers in persons with diabetes. Diabetes Metab Res Rev 2008;24:S25–30.

Hagerott BN, Blumstein AJ, McGarry LE, Cohen HM, Tenorio CA, Powell BD, et al. A bell-shaped dose–response of topical FGF-1 in accelerating dermal wound healing in aged female BALB/cByJ mice. J Proteins Proteom 2020;11:183–91.

Han G, Ceilley R. Chronic wound healing: a review of current management and treatments. Adv Ther 2017;34:599–610.

Howard MA, Asmis R, Evans KK, Mustoe TA. Oxygen and wound care: a review of current therapeutic modalities and future direction. Wound Repair Regen 2013;21:503–11.

Jabeen S, Clough ECS, Thomlinson AM, Chadwick SL, Ferguson MWJ, Shah M. Partial thickness wound: does mechanism of injury influence healing? Burns 2019;45:531–42.

Jeong SH, Zhang S, Hjort K, Hilborn J, Wu Z. PDMS-based elastomer tuned Soft, stretchable, and sticky for epidermal electronics. Adv Mater 2016;28:5830–6.

Juárez-Moreno JA, Ávila-Ortega A, Oliva AI, Avilés F, Cauich-Rodríguez JV. Effect of wettability and surface roughness on the adhesion properties of collagen on PDMS films treated by capacitively coupled oxygen plasma. Appl Surf Sci 2015;349:763–73.

Karlberg AT, Bodin A, Matura M. Allergenic activity of an air-oxidized ethoxylated surfactant. Contact Dermatitis 2003;49:241–7.

Kelly CN, Francovich J, Julmi S, Safranski D, Guldberg RE, Maier HJ, et al. Fatigue behavior of As-built selective laser melted titanium scaffolds with sheet-based gyroid microarchitecture for bone tissue engineering. Acta Biomater 2019;94:610–26.

Kimmel HM, Grant A, Ditata J. The presence of oxygen in wound healing. Wounds 2016;28:264–70.

Koh TJ, DiPietro LA. Inflammation and wound healing: the role of the macrophage. Expert Rev Mol Med 2011;13:e23.

Krisp C, Jacobsen F, McKay MJ, Molloy MP, Steinstraesser L, Wolters DA. Proteome analysis reveals antiangiogenic environments in chronic wounds of diabetes mellitus type 2 patients. Proteomics 2013;13:2670–81.

Larouche J, Sheoran S, Maruyama K, Martino MM. Immune regulation of skin wound healing: mechanisms and novel therapeutic targets. Adv Wound Care (New Rochelle) 2018;7:209–31.

Löffler MW, Schuster H, Bühler S, Beckert S. Wound fluid in diabetic foot ulceration: more than just an undefined soup? Int J Low Extrem Wounds 2013;12:113–29.

Miranda I, Souza A, Sousa P, Ribeiro J, Castanheira EMS, Lima R, et al. Properties and applications of PDMS for biomedical engineering: a review. J Funct Biomater 2021;13:2.

Nuutila K, Singh M, Kruse C, Philip J, Caterson EJ, Eriksson E. Titanium wound chambers for wound healing research. Wound Repair Regen 2016;24:1097–102.

Opdenakker G, Van Damme J, Vranckx JJ. Immunomodulation as rescue for chronic atonic skin wounds. Trends Immunol 2018;39:341–54.

Shih B, Garside E, McGrouther DA, Bayat A. Molecular dissection of abnormal wound healing processes resulting in keloid disease. Wound Repair Regen 2010;18:139–53.

Shirakami E, Yamakawa S, Hayashida K. Strategies to prevent hypertrophic scar formation: a review of therapeutic interventions based on molecular evidence. Burns Trauma 2020;8:tkz003.

Siddiqui AR, Bernstein JM. Chronic wound infection: facts and controversies. Clin Dermatol 2010;28:519–26.

Tan KT, McGrouther DA, Day AJ, Milner CM, Bayat A. Characterization of hyaluronan and TSG-6 in skin scarring: differential distribution in keloid scars, normal scars and unscarred skin. J Eur Acad Dermatol Venereol 2011;25:317–27.

Trail IA, Powell ES, Noble J. An evaluation of suture materials used in tendon surgery. J Hand Surg Br 1989;14:422–7.

Wang X, Ge J, Tredget EE, Wu Y. The mouse excisional wound splinting model, including applications for stem cell transplantation. Nat Protoc 2013;8:302–9.

Yao Z, Huang Y, Luo G, Wu J, He W. A biological membrane-based novel excisional wound-splinting model in mice (With video). Burns Trauma 2014;2:196–200.